Design of remotely located and multi-loop vibration controllers using a sequential loop closing approach

U. Ubaid[a,], S. Daley[a,], S. A. Pope[b]

[a]*Institute of Sound and Vibration Research, University of Southampton, Southampton, SO17 1BJ, UK.*
[b]*Department of Automatic Control and Systems Engineering, University of Sheffield, Sheffield, S1 3JD, UK.*

Abstract

In some applications, vibration control objectives may require reduction of levels at locations where control system components cannot be sited due to space or environmental considerations. Control actuators and error sensors for such a scenario will need to be placed at appropriate locations which are potentially remote from the points where ultimate attenuation is desired. The performance of the closed loop system, therefore, cannot be assessed simply by the measurement obtained at this local error sensor. The control design objective has to take into account the vibration levels at the remote locations as well. A design methodology was recently proposed that tackles such problems using a single-loop feedback control architecture. The work in this paper describes an extension of this control design procedure to enable the systematic design of multiple decentralised control loops. The approach is based upon sequential loop closing and conditions are provided that ensure that closed loop stability is maintained even in the event of failure in some control loops. The design procedure is illustrated through its application to a laboratory scale slab floor that replicates the problems associated with human induced vibration in large open-plan office buildings. The experimental results demonstrate the efficacy of the approach and significant suppression of the dominant low frequency modes in the floor is achieved using two independent acceleration feedback control loops.

Email addresses: u.ubaid@soton.ac.uk (U. Ubaid), s.daley@soton.ac.uk (S. Daley), s.a.pope@shef.ac.uk (S. A. Pope)

1. Introduction

Developments in actuator and sensor technologies together with faster signal processing capabilities have made active control an attractive and viable proposition for the solution of many noise and vibration problems [1]. Although active control approaches have been successfully used to suppress the local vibration levels in civil [2], marine [3] and aerospace [4] systems these application domains are often characterised by large interconnected structures with complex dynamics and distributed excitation sources. As a result the achievable performance is critically dependent on the location of the sensors and actuators and the numbers utilised should be as low as possible to avoid excessive installation costs. A number of useful methodologies to compute the optimum locations for sensors and actuators have been proposed in the literature [5–8]. However, in many instances the sensitive component or region where vibration reduction is desired is not accessible and therefore the optimal siting of sensors and actuators is not feasible. A typical example of such a problem is the vibration encountered due to aerodynamic loading on helicopter blades. The unsteady forces experienced by the rotor blades are generally transmitted at multiples of the blade passing frequency through the hub to the fuselage. Some active damping approaches that are applied directly to the rotating blades have been proposed [9], however, due to cost considerations it is more practical to apply corrective action across the gearbox at the opposite end of the propeller shaft [10] or in parallel with the attachment to the receiving structure [11]. Although the latter two approaches will reduce the locally measured fuselage vibration, the change in impedance due to this control force at the other end of the shaft can lead to an increase in blade vibration [12]. This effect has been demonstrated within the context of marine vessels in [3]. In this case, the problem arises due to the oscillatory vibration caused by the propeller blades as they pass through a non-uniform wake velocity in the fluid field. The resulting axial forces that are generated can be particularly large at rotational speeds that coincide with blade resonance and transmit through the shaft bearing leading to significant levels of vibration that propagate around the hull [13]. Similar problems of vibration enhancement away from the control point can also occur due to pinning effects in direct velocity feedback or harmonic control schemes [14, 15]. Therefore the performance of the closed loop system in such cases cannot simply be assessed in terms of the measurement obtained at the error sensor.

Robust multivariable controller design methods for vibration attenuation using centralised control schemes have been extensively presented in the literature for addressing this class of problems, see for example [6, 16]. The control design is based upon the minimisation of a desired norm, such as the $\mathcal{H}_2$ and $\mathcal{H}_\infty$ norm of the closed loop performance variables. However, vital insight into the existence of solutions and the trade-off between performance and reduction in the measured outputs is not evident to the control designer using these methods. Moreover well-established optimal control theory does not guarantee strongly stabilising controllers. Even if an internally stabilising controller could be found, the implementation of a controller that is itself unstable is not practical. As the closed loop system is only conditionally stable, any scenario that leads to a variation in gain would lead to instabilities. This can occur, for example, during commissioning and start-up as the controller gain is gradually increased to the nominal and so may pass through regions of instability [17]. One method that has been proposed to address this problem is to switch between the Youla parameterisation of a stable controller and the unstable controller until the latter is fully active [18]. There have been some methods proposed for designing stable $\mathcal{H}_\infty$ controllers [19–21] but the designs are complex and can lead to high order controllers.

For vibration control problems, it is imperative to have a degree of control and insight over the deterioration of response levels away from the error sensors. The undesirable consequences of locally optimal control actions motivated the development of a control design methodology that takes into account conflicting performance requirements and also does provide a good physical insight into the existence of vibration attenuation solutions. This geometric-based design method for controlling remote or global vibration using only local sensing and actuation was initially proposed for discrete frequency control [12] and was subsequently extended to the broad-band case under the assumption that the control loop was perfectly collocated [22]. More recently the broad-band design was generalised to the non-collocated case with non-minimum phase dynamics [23], which unlike the approach in [22] results in a stable controller. In this paper a theoretical framework for the design of multiple control loops using the geometric approach is provided, followed by an experimental implementation to validate the methodology. The method is based upon a sequential loop closing technique for the design of multiple decentralised local feedback loops.

A decentralised active control scheme is advantageous when sensor and actuator pairs are separated by large distances. Vibration mitigation of large

open plan floors in buildings and stadia using a centralised controller, for example, would require long wiring to connect a number of widely distributed sensors and actuators to the central controller. A decentralised control scheme, on the other hand, is not restricted by communication arrangements to connect the controller with the sensors and actuators. Moreover, a single sensor or actuator failure in a centralised controller could aggravate the performance at more than one location. The stability and performance of a decentralised controller, on the other hand, is less vulnerable to the failure of any single sensor or actuator in a local loop. This allows for convenient commissioning and the straightforward implementation of additional controllers on the structure.

The remainder of the article is presented as follows. The sequential loop closing approach using the geometric control design method is presented in the next section, for a generalised multivariable system. The conditions necessary for robustness of the second feedback loop in the event of failure of the first feedback loop are presented in Section 3. This serves as a design guide for robustness of any multiple loop feedback control design procedure in terms of the magnitude of the control action. In Section 4 the experimental test rig used for validating the control design is initially described, followed by the presentation of design of a two loop controller for this system. The experimental results from the controller implementation are also presented in this section, followed by some concluding remarks in Section 5.

2. Control system design

A decentralised multivariable controller is developed in this section using the sequential loop closing procedure. A generalised multivariable system relating input excitations to the vibration outputs at different points on a structure can be represented as

$$\mathbf{y}(\mathrm{j}\omega) = \begin{bmatrix} \mathbf{G}_\mathrm{c}(\mathrm{j}\omega) & \mathbf{G}_\mathrm{d}(\mathrm{j}\omega) \end{bmatrix} \begin{bmatrix} \mathbf{u}(\mathrm{j}\omega) \\ \mathbf{d}(\mathrm{j}\omega) \end{bmatrix} \tag{2.1}$$

where $\mathbf{y}(\mathrm{j}\omega)$ is an $n \times 1$ vector of vibration responses, $\mathbf{u}(\mathrm{j}\omega)$ and $\mathbf{d}(\mathrm{j}\omega)$ are the vectors of control input and disturbance excitation, respectively. $\mathbf{G}_\mathrm{c}(\mathrm{j}\omega)$ and $\mathbf{G}_\mathrm{d}(\mathrm{j}\omega)$ are matrices of control and disturbance path frequency responses, respectively. For notational convenience, the control and disturbance inputs are combined as an $m \times 1$ vector $\mathbf{f}(\mathrm{j}\omega)$ such that

$$\mathbf{y}(\mathrm{j}\omega) = \mathbf{G}(\mathrm{j}\omega)\mathbf{f}(\mathrm{j}\omega) \tag{2.2}$$

where $\mathbf{G}(\mathrm{j}\omega)$ is an $n \times m$ frequency response function matrix. The SISO frequency response function between an ith input and jth output is denoted as $g_{ji}(\mathrm{j}\omega)$. In the sequel, in order to simplify the presentation, the frequency dependence of the terms will not be denoted. However in order to avoid any ambiguity, terms that are functions of the Laplace variable, s, will be explicitly defined.

Initially a SISO controller is designed for a local feedback loop. The control signal, f_1, is generated by feeding back the local output, y_1, to a controller, k_1, as

$$f_1 = -k_1 y_1 \tag{2.3}$$

The output of this SISO loop is

$$y_1 = \sum_{i=1}^{m} g_{1i} f_i \tag{2.4}$$

Substituting (2.3) in (2.4) gives

$$y_1 = g_{11}\left(-k_1 y_1\right) + \sum_{i=2}^{m} g_{1i} f_i \tag{2.5}$$

Rearranging this expression gives

$$y_1 = \frac{1}{1 + g_{11} k_1} \left(\sum_{i=2}^{m} g_{1i} f_i \right) \tag{2.6}$$

It can be seen from (2.6) that the local vibration response can be attenuated using a controller that minimises the sensitivity function of this local feedback loop, $S_1 = [1 + g_{11} k_1]^{-1}$. Now the closed loop response of other outputs can be calculated by substituting (2.6) in (2.3) and using that as the control input, which for any general output, y_b, is given as

$$y_b = -g_{b1} k_1 \left(\sum_{i=2}^{m} \frac{g_{1i} f_i}{1 + g_{11} k_1} \right) + \sum_{i=2}^{m} g_{bi} f_i \tag{2.7}$$

After rearranging, this expression can be written as

$$y_b = \sum_{i=2}^{m} \left[1 + \left(\frac{-g_{11} k_1}{1 + g_{11} k_1} \right) \frac{g_{b1} g_{1i}}{g_{11} g_{bi}} \right] g_{bi} f_i \tag{2.8}$$

The extent of any reduction in other outputs besides the local response can be determined by expressing the local closed loop response in terms of a tuning parameter, denoted as γ_1. This parameter encapsulates the design freedom which defines the extent to which simultaneous attenuation of various outputs at discrete frequencies in the desired frequency band can be achieved. The proposed design parameter γ_1 is related to the sensitivity function of the SISO control loop according to

$$\gamma_1 W_1 B_1 = S_1 - 1 = \frac{-g_{11}k_1}{1 + g_{11}k_1} \tag{2.9}$$

where B_1 is the frequency response of an all-pass transfer function formed from the right half plane zeros of $g_{11}(s)$, such that $g_{11}(s) = \hat{g}_{11}(s)B_1(s)$, where $\hat{g}_{11}(s)$ is the minimum phase counterpart of $g_{11}(s)$; and W_1 is the frequency response of a weighting filter chosen to suppress control spillover at out-of-band frequencies. This is required to avoid excitation of unmodelled high frequency residual modes which may lead to instabilities. A low order filter is recommended in order to avoid large phase changes in the design frequency bandwidth. However, higher modal densities in the plant may necessitate higher order filters for sufficient roll-off of controller gain. Direct substitution of (2.9) in (2.8) results in

$$y_b = \sum_{i=2}^{m} \left[1 + \gamma_1 W_1 B_1 \frac{g_{b1}g_{1i}}{g_{11}g_{bi}}\right] g_{bi} f_i \tag{2.10}$$

which is the closed loop response due to the closing of the first control loop. Using (2.10), the partial closed loop transfer function matrix relating the remaining inputs to the outputs can be written as

$$\mathbf{y} = \mathbf{H}\mathbf{f}^{(1)} \tag{2.11}$$

where $\mathbf{f}^{(m)}$ denotes the mth row of $\mathbf{f}$ removed and $\mathbf{H}$ is $n \times (m-1)$. The individual transfer function element between the jth output and the ith input is given as

$$h_{ji} = \left[1 + \gamma_1 W_1 B_1 \frac{g_{j1}g_{1i}}{g_{11}g_{ji}}\right] g_{ji} \tag{2.12}$$

The closed loop response of a single output to excitation by a disturbance input can be attenuated using control input f_1 if the magnitude of the partial closed loop transfer function that relates this disturbance input and output

is minimised, relative to the open loop case. For example, an output y_{e} due to disturbance input f_{d} can be attenuated using control input f_1 if

$$\left|\frac{h_{\mathrm{ed}}}{g_{\mathrm{ed}}}\right| < 1 \tag{2.13}$$

Substituting (2.12) in (2.13) gives

$$\left|1 + \gamma_1 W_1 B_1 \frac{g_{\mathrm{e1}} g_{\mathrm{1d}}}{g_{11} g_{\mathrm{ed}}}\right| < 1 \tag{2.14}$$

or alternatively written as

$$|\gamma_1 + U_{\mathrm{ed}}| < |U_{\mathrm{ed}}| \tag{2.15}$$

where

$$U_{\mathrm{ed}} = \frac{g_{11} g_{\mathrm{ed}}}{W_1 B_1 g_{\mathrm{e1}} g_{\mathrm{1d}}} \tag{2.16}$$

Inequality (2.15) evaluated at a discrete frequency ω_0 represents a region inside a circle with centre $-U_{\mathrm{ed}}$ and radius $|U_{\mathrm{ed}}|$, in a complex γ_1-plane. Similarly, the reduction in the closed loop response between any other output and disturbance input pair can be portrayed as a circular region in the same plane. The optimal value for the design parameter to achieve attenuation in a particular output has to be then selected from inside the circular region near its centre. A set of design parameter values for discrete frequencies within a frequency band are selected and this set is then interpolated using any suitable interpolation algorithm to obtain a continuous and causal design parameter transfer function $\gamma_1(s)$. The existence of a stable function that interpolates this set of γ_1 values is determined from the positive definiteness of the Pick matrix [24]. Additionally, an optimisation of the γ_1 values within an acceptable attenuation performance can be performed using Linear Matrix Inequalities as has been described in [22]. The final optimised set of complex points can then be interpolated using the Nevanlinna-Pick interpolation algorithm [25] to obtain a continuous and causal design parameter transfer function $\gamma_1(s)$, using a similar approach to [22]. Additional parameters in Nevanlinna-Pick interpolation can be tuned to satisfy various frequency response specifications as described in [22, 26]. A controller that achieves the desired vibration attenuation performance as encapsulated by this design parameter can be obtained by rearranging (2.9) to give

$$k_1(s) = \frac{-\gamma_1(s) W_1(s)}{\left[1 + \gamma_1(s) W_1(s) B_1(s)\right] \hat{g}_{11}(s)} \tag{2.17}$$

It can be observed from (2.9) that since $W_1(s)B_1(s)$ is stable, selecting $\gamma_1(s)$ to be a stable function guarantees closed loop stability, provided there are no unstable pole-zero cancellations between $g_{11}(s)$ and $k_1(s)$. In addition, since $\hat{g}_{11}(s)$ has no RHP zeros a controller given by (2.17) guarantees strong stabilization if the Nyquist contour of $\gamma_1 W_1 B_1$ does not enclose the (-1,0) point. This follows from the form of the controller structure given in (2.17) since this is equivalent to a closed loop feedback system having an open-loop frequency response function of $\gamma_1 W_1 B_1$. If these conditions are satisfied, the partial closed loop system dynamics with the first control loop closed can be examined using (2.11), which is subsequently used for the design of the next local feedback controller. It should be noted that U_{ed} given by (2.16) is a dimensionless quantity which, as noted in earlier fundamental control research, provides a useful measure for the severity of the trade-off between stability robustness and disturbance attenuation [27]. This trade-off will be severe for frequencies at which U_{ed} is very large or very small, which is the case in flexible structures and is attributed to their lightly damped zeros [28]. In the context of the design procedure developed here this will manifest itself for the case of a very small U_{ed} as a very small circle close to the origin meaning that significant reductions in local vibration can only be achieved at the expense of enhancement elsewhere on the structure. Conversely when U_{ed} is very large then significant reductions at the remote point will only be achieved at the expense of local enhancement.

The main steps in the design of the second feedback control system are similar to the first control loop, however, instead of the open loop system dynamics the partial closed loop system dynamics with the first loop closed are used. The equivalent design parameter γ_2 in this case is related to the closed loop dynamics of the local feedback loop according to

$$\gamma_2 W_2 B_2 = \frac{-h_{22}k_2}{1 + h_{22}k_2} \tag{2.18}$$

where W_2 is a weighting filter to suppress control spillover at out-of-band frequencies and B_2 is an all-pass transfer function formed from the RHP zeros of $h_{22}(s)$. In a similar fashion to the vibration attenuation condition described by inequality (2.15) as a circular region in a γ_1-plane, the reduction in the closed loop response using this second feedback controller between any particular output and disturbance input pair can be described as a circular region in a complex γ_2-plane. The controller that achieves the desired

attenuation performance is implemented as

$$k_2(s) = \frac{-\gamma_2(s)W_2(s)}{[1+\gamma_2(s)W_2(s)B_2(s)]\,\hat{h}_{22}(s)} \tag{2.19}$$

The conditions necessary for controller (2.19) to be strongly stabilising are equivalent to those described for controller (2.17).

The above control design can be extended to include even more local feedback loops. Every time a local feedback loop is designed, the subsequent partial closed loop dynamics can be computed as in (2.11) and the design steps described above for the second feedback loop can be repeated for any number of loops.

3. Integrity to the failure of individual loops

One of the disadvantages of the sequential loop closing design is that the stability of individual control loops is not guaranteed when other inner feedback loops fail. It is desirable for a decentralised control system to have integrity so that individual controllers can be switched on or off without complete loss of vibration attenuation. In this section, the necessary conditions to satisfy closed loop stability of the control system in the face of failure of individual control loops will be formulated.

The controller $k_2(s)$ for the second feedback loop is designed for the partial closed loop system in (2.11) assuming that a stable feedback controller $k_1(s)$ is already implemented. Therefore the stability of the second feedback loop is determined by the stability of $\gamma_2(s)$ as given in (2.18). However in this case if the first feedback loop fails then this controller, which is implemented in terms of the partial closed loop dynamics, may not still ensure closed loop stability. Since there can be no unstable pole-zero cancellations between $g_{22}(s)$ and $k_2(s)$, the closed loop stability of the second control loop in the event of failure of the inner loop can be determined by examining the stability of

$$\Gamma_2(s) = \frac{-g_{22}(s)k_2(s)}{1+g_{22}(s)k_2(s)} \tag{3.1}$$

As the controller $k_2(s)$ is itself implemented in terms of a pre-designed $\gamma_2(s)$, the expression from (2.19) is substituted into (3.1). After simplifying this

gives

$$\Gamma_2(s) = \frac{\gamma_2(s)W_2(s)\dfrac{g_{22}(s)}{\hat{h}_{22}(s)}}{1+\gamma_2(s)W_2(s)B_2(s)\left[1-\dfrac{g_{22}(s)}{h_{22}(s)}\right]} \tag{3.2}$$

As $\hat{h}_{22}(s)$ is minimum phase, the numerator of (3.2) is stable. So the closed loop stability is dependent upon the roots of the denominator of (3.2). By noting that $h_{22}(s) = \hat{h}_{22}(s)B_2(s)$, the denominator of (3.2) can be denoted as

$$D(s) = 1+\gamma_2(s)W_2(s)\left[\frac{h_{22}(s)-g_{22}(s)}{\hat{h}_{22}(s)}\right] \tag{3.3}$$

It can be seen in (3.3) that $D(s)$ has no open loop right half plane poles, therefore, as per Cauchy's argument principle, the total number of encirclements of the origin as $D(s)$ traverses the Nyquist D-contour in a clockwise direction is equal to the number of right half plane zeros of $D(s)$. Thus, (3.1) is stable if the Nyquist contour of $D(s)$ does not encircle the origin. The robustness of the second control loop to the failure of the first control loop can therefore be ensured if the Nyquist contour of (3.4) does not enclose the (-1+j0) point.

$$D(s)-1 = \gamma_2(s)W_2(s)B_2(s)\left[1-\frac{g_{22}(s)}{h_{22}(s)}\right] \tag{3.4}$$

3.1. Robustness of sequential loops

A general condition for robustness of a single control loop can be formulated by relating its design parameter with that of another control loop. By using the small gain theorem to satisfy the Nyquist stability criterion of (3.4), this has been derived for the design parameters of the first and second control loops from Section 2 as a guide in Appendix A. By extension a general conclusion concerning the robustness of a control loop to the failure of an inner control loop can be stated as a design rule for any sequential loop closing procedure as follows.

Theorem 3.1. *The robustness of an outer loop to the failure of an inner loop can be guaranteed if the following inequality is satisfied*

$$\left|\gamma_p - \left(\frac{1}{M_q^2-1}\right)A_{pq}\right| \leq \frac{M_q}{\left(M_q^2-1\right)}\left|A_{pq}\right| \qquad \forall\omega \tag{3.5}$$

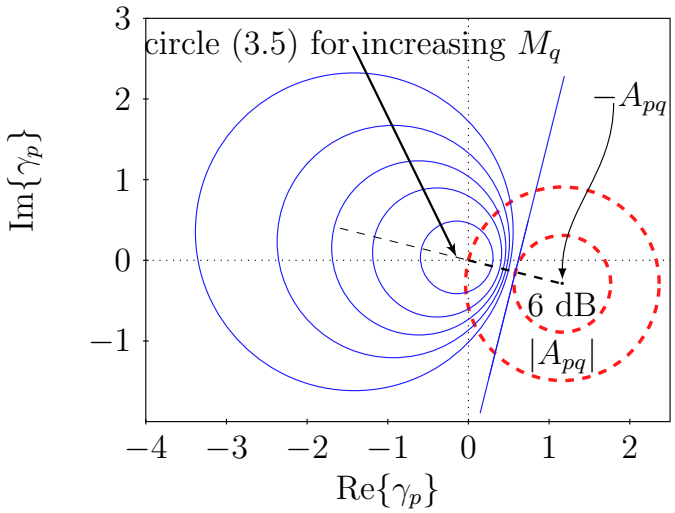

Figure 1: The region in the γ_p-plane for selection of the design freedom parameter, that ensures robustness to failure, reduces as M_q increases, as per inequality (3.5). The larger red dashed circle denotes the region as per inequality (3.7) where $-A_{pq}$ as given by (3.6) is its centre. The smaller red dashed circle marks the boundary of 6 dB attenuation in the response between the second error sensor and the second loop control force.

where $M_q \approx \sup_{\omega} |\gamma_q(\mathrm{j}\omega)|$, γ_q *and* γ_p *are the design parameters associated with the outer and inner feedback loops, respectively and*

$$A_{pq} = \frac{g_{pp} g_{qq}}{W_p B_p g_{pq} g_{qp}} \tag{3.6}$$

Proof. Refer to Appendix A. □

Corollary 3.1. *If the control action due to the inner loop* (u_p) *causes more than 6 dB attenuation in the response between the output of the error sensor of the outer loop* (y_q) *and the control input of the outer loop* (u_q) *then there can be no disturbance attenuation controller for the outer loop that can satisfy the robust stability constraint.*

Proof. The term $-A_{pq}$ in (3.6) evaluated at a discrete frequency is the centre of a circle in the γ_p-plane that corresponds to attenuation in output at the second controller error sensor resulting from control action in the first feedback loop for any primary excitation applied at the point of application of the second loop control force. The region in the γ_p-plane that denotes

this specific attenuation is plotted as a red dashed circle in Figure 1 and it is given by the inequality

$$|\gamma_p + A_{pq}| \leq |A_{pq}| \tag{3.7}$$

Assuming that the maximum peak magnitude M_q of the design parameter γ_q is already known, then the conditions for robustness can be formulated as different regions in a γ_p-plane with respect to the circle (3.7). Comparing the two circles given by inequalities (3.5) and (3.7), it can be seen that the centre and radius of circle (3.5) are equal to the centre and radius of circle (3.7) scaled by factors $\left[M_q^2 - 1\right]^{-1}$ and $M_q\left[M_q^2 - 1\right]^{-1}$, respectively. For disturbance attenuation purposes, only values of $M_q \geq 1$ are of interest. If $M_q > 1$, then the circle (3.5) encloses the origin and the point $-A_{pq}$ lies outside this circle. As M_q increases, the centre of this circle approaches the origin and its size reduces, as illustrated in Figure 1. Although there is an overlap between circle (3.5) (blue solid circle) and circle (3.7) (red dashed circle), this region of overlap reduces as M_q increases. The maximum overlap between these two circles can be found by substituting $M_q = 1$ in (A.8), which results in a perpendicular bisector of the line joining $-A_{pq}$ with the origin. For robust stability of both control loops, a value for γ_p will have to be selected at this frequency from a region that lies inside the circle (3.5). This circle for $M_q \geq 1$ excludes at least a region of 6 dB attenuation in the response from the second loop control force to the second loop error sensor due to the action of the first control loop. □

Remark As the peak magnitude of $\gamma_q(\mathrm{j}\omega)$ increases, the region in the γ_p-plane available for controller implementation reduces and this imposes an additional constraint on the implementation of a controller for the first loop. Predictably, selection of γ_p from inside these circles for increasing values of M_q results in very low controller gain at these frequencies. The peak magnitude M_q gives the worst case scenario for selection of γ_p such that the second control loop is robust to the failure of the first control loop. A less conservative approach would be to instead use the actual magnitude of $\gamma_q(\mathrm{j}\omega)$ to determine the feasible regions in the γ_p-plane for robust stability. This would allow selection of γ_p from a larger region as compared to the more conservative small gain approach.

It should also be noted that the robustness to failure is a condition on the selection of design freedom parameter for the inner feedback loop in terms

of the magnitude of the design freedom parameter for the outer feedback loop. However, selection of the latter parameter itself depends on the partial closed loop transfer function due to the first feedback loop. In the absence of an estimate for the magnitude of the local closed loop transfer function in the design frequency band, this method would require an iterative procedure for verification of robustness. In the case of a third outer feedback loop, if the second loop is robust to the failure of the first loop, then the stability of the third loop is assessed for the simultaneous failure of the first and second loops, as well as their individual failures. Therefore, it can be seen that as an additional control loop is added the number of conditions that need to be checked for robust stability with integrity increases by a factor of 2.

4. Experimental verification

4.1. Experimental set up

The multivariable control design procedure proposed in this paper is illustrated through its application to a laboratory scale slab floor, shown in Figure 2, that replicates the problems associated with human induced vibration in large open-plan office buildings [29]. The development of stronger but lighter materials has allowed the ready construction of large open-plan building floors. These lightweight structures unfortunately exhibit both lower damping and natural frequencies which are readily excited by periodic human motion or operation of indoor equipment and machinery. Although this is not a safety concern, vibration mitigation is an ongoing area of research amongst the civil and structural engineering community due to vibration serviceability requirements [2].

The slab structure presented here has been previously used for the study of active vibration mitigation techniques in floor structures due to human induced excitations [30, 31]. The total length of this simply-supported slab is 11.2 m which includes 200 mm overhangs over each edge support. It is 2.0 m wide, 275 mm thick and weighs approximately 15 tonnes [29]. The first mode of vibration has a natural frequency around 4.4 Hz, the second bending mode occurs around 16.7 Hz while the third mode is a torsional mode which occurs around 26.2 Hz. The objective of the control design for this application is to minimise the peak levels at low frequencies that are prone to excitation by the harmonics of walking, running, jumping, etc. Although the dynamics are less complex than encountered in many buildings

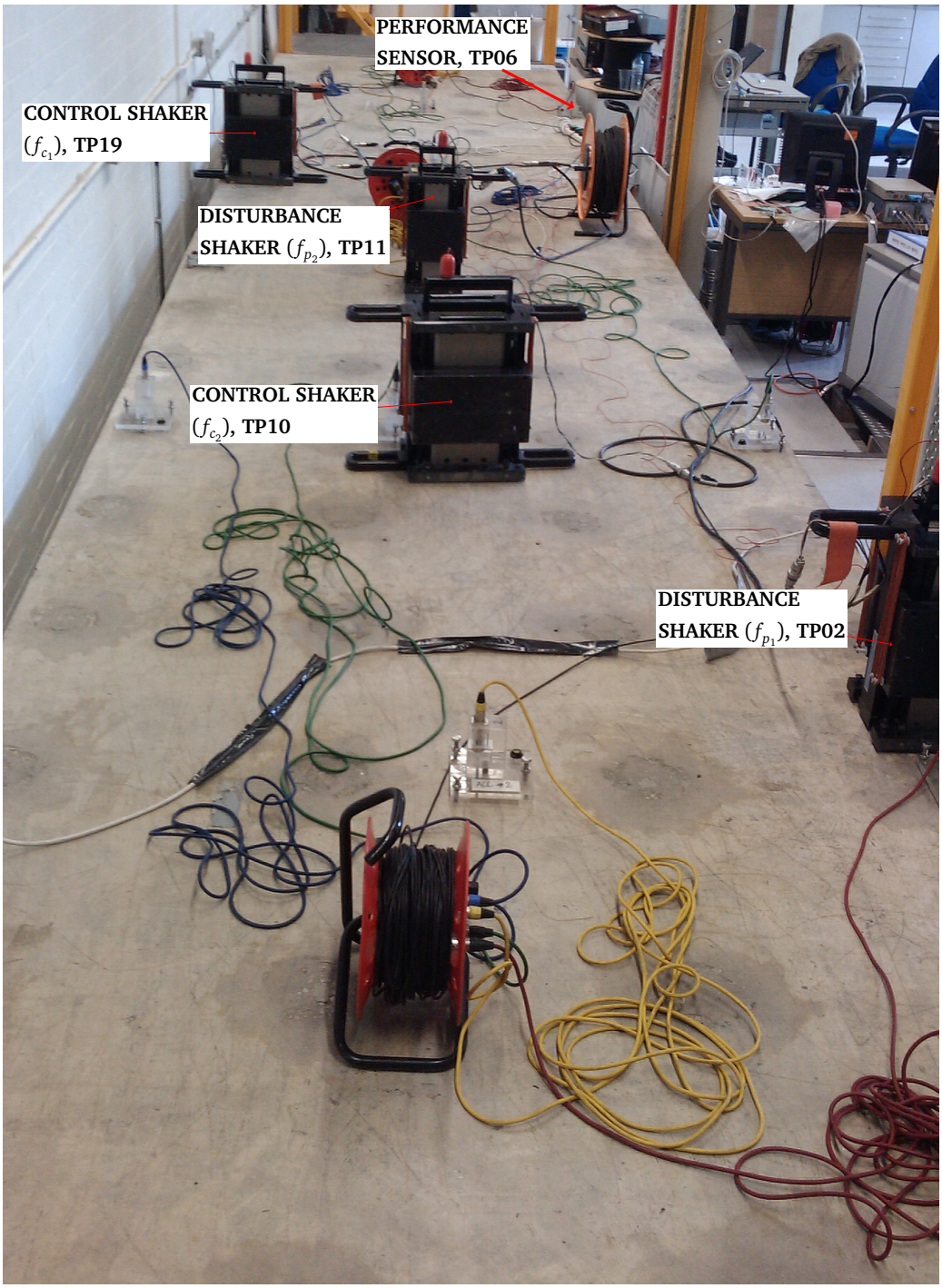

Figure 2: View of the laboratory set-up from one end showing the locations of the two control shakers, the two disturbance shakers and the performance measurement sensor at TP06

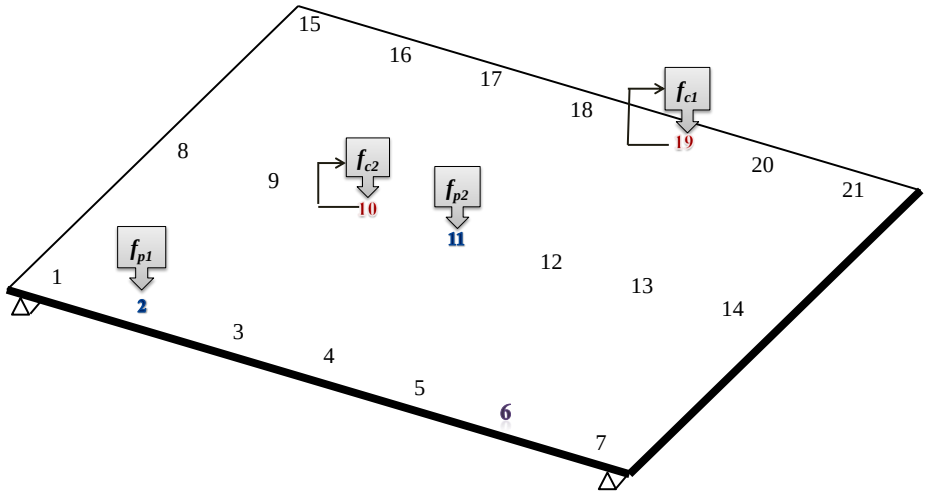

Figure 3: Schematic of the concrete slab showing the location of the excitation shakers (f_{p_1} and f_{p_2}) and the control shakers (f_{c_1} and f_{c_2}) on the structure, the acceleration is also measured at test point 6 (TP06) for remote performance evaluation

this experimental facility serves as a realistic structure to illustrate the design methodology proposed in this paper.

4.2. Measurement and performance test points

The first bending mode of the slab can be excited by a suitable force near its mid-span. This is achieved using a primary excitation shaker at test point 11 (TP11), denoted as f_{p_2} in Figure 3. The second bending and torsional modes are excited using a disturbance shaker at TP02, denoted as f_{p_1} in Figure 3. The first feedback loop is designed for a control shaker placed at TP19, denoted as f_{c_1} in Figure 3, as it can attenuate the torsional mode effectively from this location. A suitable location for the second control shaker, denoted as f_{c_2} in Figure 3, is chosen at TP10 because it can affect the first and second bending mode of the slab appropriately. An additional remote point at TP06 is chosen for performance evaluation of the remote vibration controller since all three modes are readily visible at this location. The open loop frequency response between the inputs and outputs can be obtained by feeding uncorrelated random excitation to the four shakers and taking measurements of the accelerometers at the five test points. A decentralised multivariable controller for the two control shakers is designed in this section using the sequential loop closing procedure. Initially, a SISO controller is

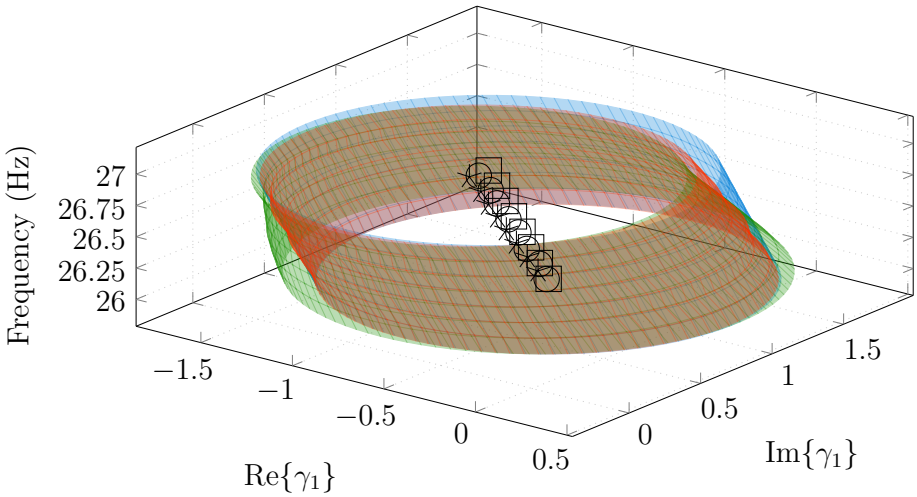

Figure 4: Regions in the γ_1-plane around the torsional mode frequency describing the reduction in output at TP06 (centre of circle $\circ$), TP02 (centre of circle $\star$) and TP19 (centre of circle $\square$)

designed for the shaker at TP19 for attenuation around the torsional mode frequency of the structure. The partial closed loop system dynamics subsequently obtained are then used to design a controller for the shaker at TP10.

4.3. Feedback controller at TP19

The acceleration measurement at TP19 is used as a feedback signal in order to generate a control signal which drives the shaker at this position. Initially, an LTI model is determined from the measured frequency response for the open loop control path. This is a 6th order transfer function model approximation which has one non-minimum phase zero. Secondly, in order to ensure suppression of control energy outside the torsional mode frequency band a suitable weighting filter is selected here as an 8th order bandpass butterworth filter with cut-on frequency 19.9 Hz and cut-off frequency 39.4 Hz. The reduction in closed loop response between the output at any test point and a disturbance input at any test point can be portrayed as a circular region in the complex γ_1-plane using inequality (2.15). The circles describing attenuation at TP19, TP02 and TP06 for certain frequencies around the torsional mode frequency are shown in Figure 4. It can be seen that the

regions completely overlap which indicates that simultaneous attenuation in the output at the three test points is possible using this control input.

It was shown previously using the geometric approach that for any structure near a resonant frequency the circles that represent vibration reduction always overlap, provided it is not for an output that lies at a node corresponding to that mode [32]. This result of course is intuitively true for the reduction of a lightly damped mode where modal density is low. The general design framework allows for strong global stability, fault tolerance and suppression across specific frequency spans away from resonance. The optimal values for the design parameter can be selected from inside these circular regions near their centre for global attenuation. The set of optimal values of the design parameter is then interpolated using the Nevanlinna-Pick interpolation algorithm, as noted in Section 2. This transfer function is then used to realise a controller as given by (2.17) which when implemented will achieve the desired reduction in the closed loop response between the disturbance input at TP02 and the outputs at TP19, TP02 and TP06. The partial closed loop system dynamics with the first control loop closed is estimated using (2.11) and (2.12), which is subsequently used for the design of a second feedback controller at TP10.

4.4. Feedback controller at TP10

The main steps in the design of a feedback control system at TP10 are similar to the first control loop. The design parameter for this loop is related to the local partial closed loop transfer function as in (2.18). An LTI model is identified for the local control path from the control shaker input signal to the error accelerometer at TP10, using the calculated partial closed loop frequency response. This gives a 4th order transfer function model which has one non-minimum phase zero. It is intended that the second controller at TP10 achieves attenuation around the first and second natural frequencies of the structure. A major concern using active vibration control in this application is the dynamics of the actuators which can adversely affect the system performance and stability margins, especially when the resonant frequency of the inertial mass of the shaker is close to the structural resonance that is desired to be controlled. In this case, the natural frequency of the actuator, estimated to be around 1.3 Hz, can reduce stability margins. A suitable weighting filter to suppress control spillover is therefore selected as a bandpass butterworth filter with a low cut-on frequency of 2 Hz and a high cut-off frequency of 25.7 Hz.

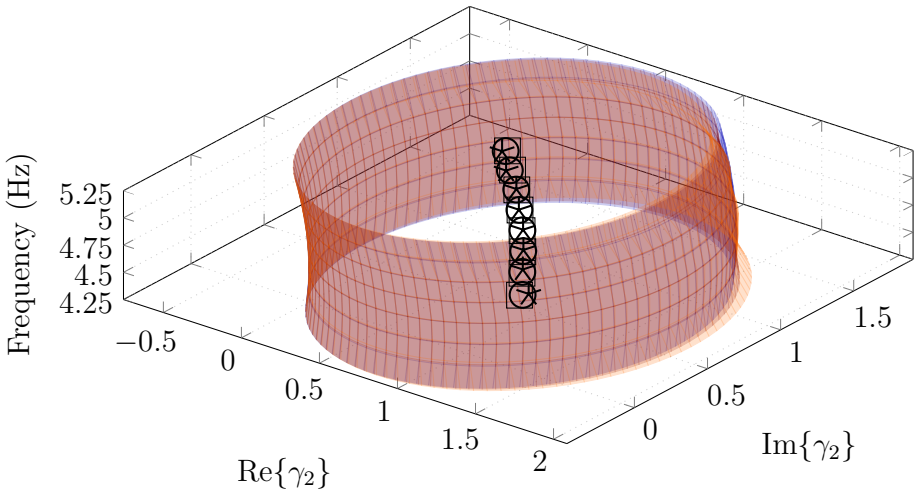

Figure 5: Regions in the γ_2-plane near the second natural frequency describing the reduction in output at TP06 (centre $\star$), TP11 (centre $\circ$) and TP10 (centre $\square$)

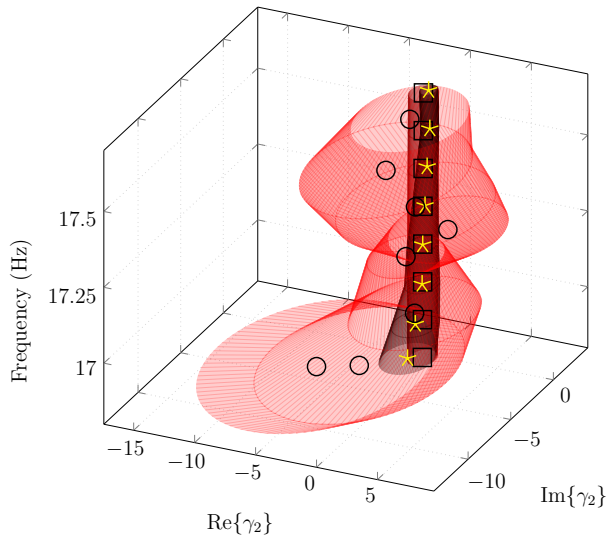

Figure 6: Regions in the γ_2-plane in the frequency band near the second natural frequency describing the reduction in output at TP06 (centre $\star$), TP11 (centre $\circ$) and TP10 (centre $\square$)

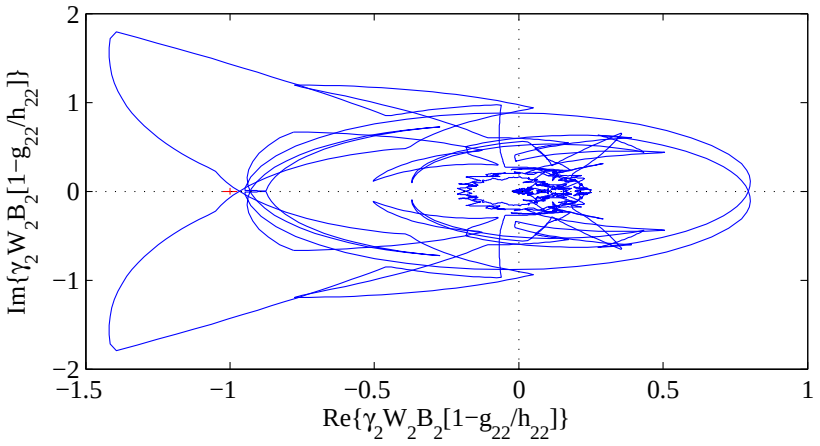

Figure 7: Nyquist plot of the term given in (3.4) which determines the robustness of the second loop when inner loop fails

In a similar fashion to the vibration attenuation conditions for the first feedback loop, vibration attenuation at TP06, TP10 and TP11 can be portrayed as circular regions in a γ_2-plane. This region for frequencies near the first bending mode frequency, as shown in Figure 5, almost completely overlap for all the test points. However, for frequencies near the second resonance the circles representing attenuation at TP11 do not overlap with the circles of the other test points, as seen in Figure 6. This is due to the presence of a node near TP11 for this mode. Therefore, the optimal values for the design parameter are selected from near the centre of the circle that represents attenuation at TP10. This set of optimal values is then interpolated using the Nevanlinna-Pick interpolation algorithm to obtain the design parameter transfer function which is then used to implement the controller using (2.19). This controller is strongly stabilising and its robustness to failure of the first feedback loop can be checked by plotting the Nyquist contour of (3.4) which is shown in Figure 7. It can be seen that the Nyquist contour does not enclose the critical point which signifies that this controller will be robust to failure of the first feedback loop.

4.5. Results and Discussion

The controllers that were developed in Sections 4.3 and 4.4 were produced as continuous-time transfer functions. These are converted to a discrete-time function using a first order hold approximation with a sampling frequency

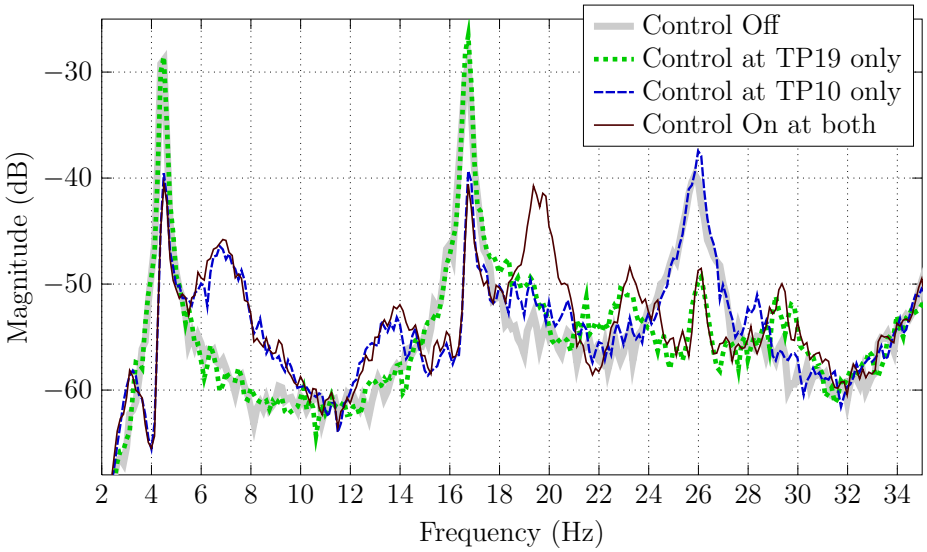

Figure 8: Power spectral density of the output at TP06, open loop (thick shaded), partial closed loop with control action at only TP19 (dotted) and only TP10 (dashed), and both loops closed (thin solid)

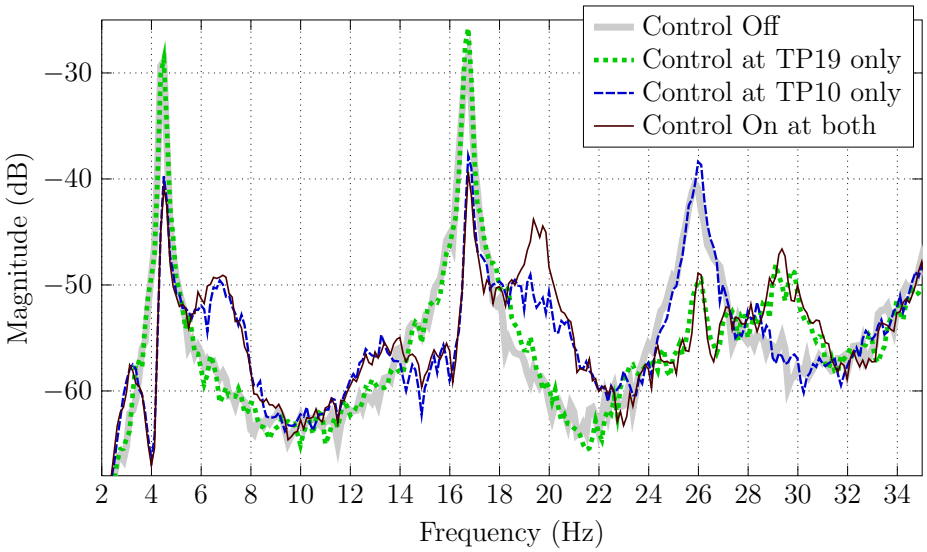

Figure 9: Power spectral density of the output at TP02, open loop (thick shaded), partial closed loop with control action at only TP19 (dotted) and only TP10 (dashed), and both loops closed (thin solid)

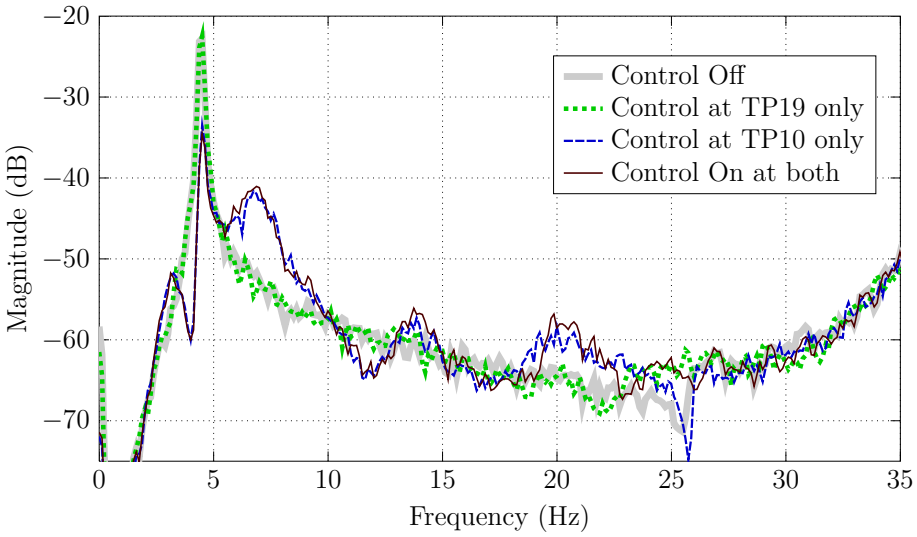

Figure 10: Power spectral density of the output at TP11, open loop (thick shaded), partial closed loop with control action at only TP19 (dotted) and only TP10 (dashed), and both loops closed (thin solid)

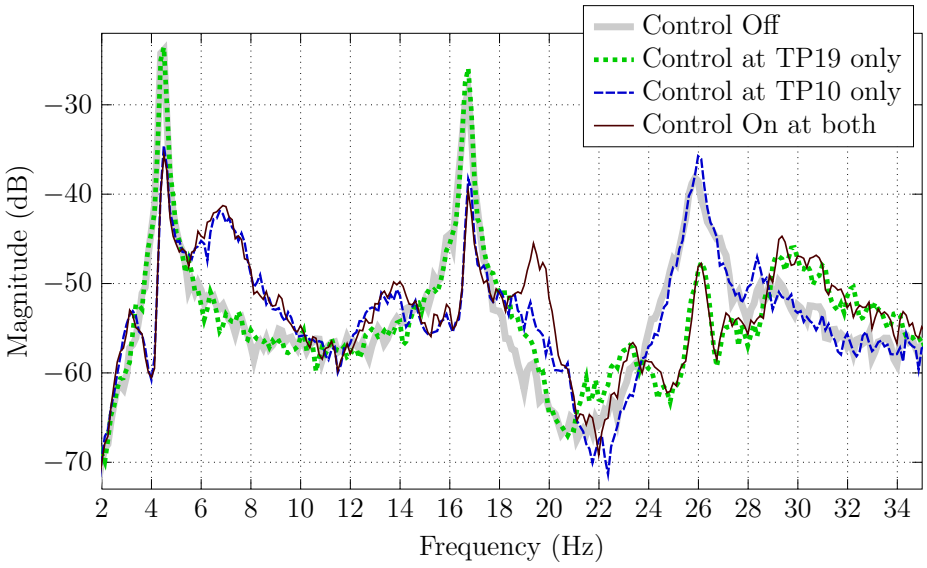

Figure 11: Power spectral density of the output at TP19, open loop (thick shaded), partial closed loop with control action at only TP19 (dotted) and only TP10 (dashed), and both loops closed (thin solid)

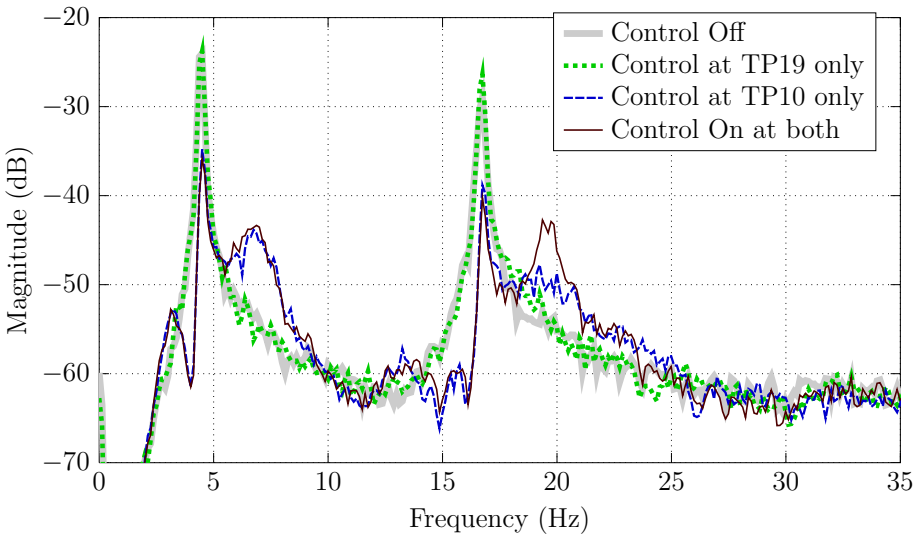

Figure 12: Power spectral density of the output at TP10, open loop (thick shaded), partial closed loop with control action at only TP19 (dotted) and only TP10 (dashed), and both loops closed (thin solid)

of 2000 Hz prior to implementation in the laboratory using dSPACE real time interface hardware. Random excitation is fed to both the disturbance shakers at TP02 and TP11 and the output of the accelerometers at the relevant test points is recorded for three different runs of experiments. In the first run, control at TP10 is switched off and only the control shaker at TP19 is operational. It can be seen from the power spectral density plots in Figures 8, 9 and 11 that there is a reduction of approximately 10 dB in the response levels at TP06, TP02 and TP19 around the torsional mode frequency. For the second run of experiments, the control shaker at TP10 is turned on and the one at TP19 is switched off. In this case the response levels at TP06, TP02, TP19 and TP10 reduce by around 15 dB near the frequency of the second bending mode as seen in Figures 8, 9, 11 and 12. There is also a reduction of more than 10 dB in response levels at all the test points around the frequency of the first bending mode, which can also be seen for TP11 in Figure 10. In the final run of experiments, the control shaker at TP19 is switched on followed by the control shaker at TP10. The closed loop system remains stable for this configuration even when one of the controllers is switched off. This demonstrates the robustness of both

control loops to the failure of individual loops. The PSD of the outputs at all test points for both controllers switched on shows an overall reduction that is similar to the combined attenuation of the two individual controllers. There is some evidence of minor waterbed effects around 7 and 20 Hz that could be addressed with further refinement of the controller. For example, careful selection of the design freedom parameter at these frequencies could be undertaken at the expense of a higher order controller. However the levels are not significant in the context of this application and remain an order of magnitude below the uncontrolled peak.

5. Conclusion

A strongly stabilising decentralised multivariable control design procedure using a sequential loop closing approach has been presented in this paper. It is well known that the interaction between SISO control loops in a coupled multivariable system can cause instabilities if any single loop fails. It has been shown here that the integrity of individual control loops can be satisfied as certain conditions in terms of the magnitude and values of a design freedom parameter. The maximum peak magnitude of the design parameter associated with a specific control loop can be used to establish its robustness to the failure of another control loop. Conversely, this can also be used to select values of the design parameter for the other control loops. Experimental results on a floor slab structure shows the efficacy of this method for the design of multiple local feedback loops. The first control loop at a test point is designed for the attenuation of vibration levels near the torsional mode resonant frequency. The subsequent prediction of partial closed loop system dynamics are then used to design a second controller at a different test point to attenuate the levels near the first and second bending mode resonant frequencies. The performance of this multivariable controller is validated using measurement levels at a remote test point. The controller is also shown to be robust to the failure of any single individual feedback loop.

Acknowledgement

The experimental work was supported through the EPSRC responsive mode grant entitled "Active Control of Human Induced Vibration" (Ref: EP/H009825/1). This support is gratefully acknowledged as is the assistance

of Dr Donald Nyawako and Professor Paul Reynolds when undertaking the experimental work. The authors would also like to thank the reviewers of the original manuscript for their helpful suggestions which greatly improved the presentation.

Appendix A Design freedom for loop failure

As per the small gain theorem, the Nyquist contour of (3.4) will not enclose the -1 point if

$$\left\| \gamma_2 W_2 B_2 \left[1 - \frac{g_{22}}{h_{22}} \right] \right\|_\infty \leq 1 \tag{A.1}$$

Denoting the maximum peak magnitude of $\gamma_2(\mathrm{j}\omega)$ as M_2, from the properties of vector norms, the product of the $\infty-$norms is greater than or equal to the $\infty-$norm of the products

$$\left\| \gamma_2 W_2 B_2 \left[1 - \frac{g_{22}}{h_{22}} \right] \right\|_\infty \leq M_2 \left\| \left[1 - \frac{g_{22}}{h_{22}} \right] \right\|_\infty \tag{A.2}$$

Consequently, the condition in (A.1) will be satisfied if

$$M_2 \left\| \left[1 - \frac{g_{22}}{h_{22}} \right] \right\|_\infty \leq 1 \tag{A.3}$$

Dividing both sides of inequality by M_2 and substituting h_{22} from (2.12) gives

$$\left\| \left[1 - \frac{g_{22}}{\left(1 + \gamma_1 W_1 B_1 \dfrac{g_{21} g_{12}}{g_{11} g_{22}} \right) g_{22}} \right] \right\|_\infty \leq \frac{1}{M_2} \tag{A.4}$$

this can simplified as

$$\left\| \left[1 + \frac{g_{11} g_{22}}{\gamma_1 W_1 B_1 g_{21} g_{12}} \right]^{-1} \right\|_\infty \leq \frac{1}{M_2} \tag{A.5}$$

or alternatively written as

$$\left| \left[1 + \frac{g_{11} g_{22}}{\gamma_1 W_1 B_1 g_{21} g_{12}} \right]^{-1} \right| \leq \frac{1}{M_2} \qquad \forall \omega \tag{A.6}$$

As both sides of inequality are positive, inversion leads to

$$\left| 1 + \frac{g_{11} g_{22}}{\gamma_1 W_1 B_1 g_{21} g_{12}} \right| \geq M_2 \qquad \forall \omega \tag{A.7}$$

which is rearranged as

$$\left|\gamma_1 + \frac{g_{11}g_{22}}{W_1 B_1 g_{21} g_{12}}\right| \geq M_2 \left|\gamma_1\right| \qquad \forall\omega \tag{A.8}$$

For clarity denote

$$A_{12} = \frac{g_{11}g_{22}}{W_1 B_1 g_{21} g_{12}} \tag{A.9}$$

Substituting (A.9) in (A.8) gives

$$\left|\gamma_1 + A_{12}\right| \geq M_2 \left|\gamma_1\right|$$

Squaring both sides

$$\begin{aligned}
\left(\gamma_1 + A_{12}\right)\left(\overline{\gamma}_1 + \overline{A}_{12}\right) &\geq M_2^2 \gamma_1 \overline{\gamma}_1 \\
\gamma_1\overline{\gamma}_1 - M_2^2\gamma_1\overline{\gamma}_1 + \gamma_1\overline{A}_{12} + \overline{\gamma}_1 A_{12} &\geq -A_{12}\overline{A}_{12} \\
\left[M_2^2 - 1\right]\gamma_1\overline{\gamma}_1 - \gamma_1\overline{A}_{12} - \overline{\gamma}_1 A_{12} &\leq A_{12}\overline{A}_{12}
\end{aligned}$$

Dividing by $[M_2^2 - 1]$

$$\begin{aligned}
\gamma_1\overline{\gamma}_1 - \frac{\overline{A}_{12}}{[M_2^2-1]}\gamma_1 - \frac{A_{12}}{[M_2^2-1]}\overline{\gamma}_1 &\leq \frac{A_{12}\overline{A}_{12}}{[M_2^2-1]} \\
\gamma_1\overline{\gamma}_1 - \frac{\overline{A}_{12}}{[M_2^2-1]}\gamma_1 - \frac{A_{12}}{[M_2^2-1]}\overline{\gamma}_1 + \frac{\left|A_{12}\right|^2}{[M_2^2-1]^2} &\leq \frac{A_{12}\overline{A}_{12}}{[M_2^2-1]} + \frac{\left|A_{12}\right|^2}{[M_2^2-1]^2} \\
\left|\gamma_1 - \frac{A_{12}}{[M_2^2-1]}\right|^2 &\leq \frac{A_{12}\overline{A}_{12}\left[M_2^2-1\right] + (A_{12})(\overline{A}_{12})}{[M_2^2-1]^2} \\
\left|\gamma_1 - \frac{A_{12}}{[M_2^2-1]}\right|^2 &\leq \frac{M_2^2\left|A_{12}\right|^2}{[M_2^2-1]^2}
\end{aligned}$$

Taking square root of the above inequality gives

$$\left|\gamma_1 - \frac{A_{12}}{[M_2^2-1]}\right| \leq \frac{M_2\left|A_{12}\right|}{[M_2^2-1]}$$

Finally, substituting A_{12} back from (A.9) yields

$$\left|\gamma_1 - \left(\frac{1}{M_2^2 - 1}\right)\frac{g_{11}g_{22}}{W_1 B_1 g_{12}g_{21}}\right| \leq \frac{M_2}{(M_2^2 - 1)}\left|\frac{g_{11}g_{22}}{W_1 B_1 g_{12}g_{21}}\right| \qquad \forall\omega \quad \text{(A.10)}$$

This inequality denotes the condition on the design freedom parameter γ_1 for the first feedback loop in terms of the maximum peak magnitude M_2 of the design freedom parameter for the second feedback loop.

References

References

[1] Tokhi, O and Veres, S, Active Sound and Vibration Control: Theory and Applications, *IEE Control Engineering Series* **62**, 2002

[2] Nyawako, DS and Reynolds, P, Technologies for the mitigation of human induced vibrations in civil engineering structures, *The shock and vibration digest.* **39**(6): 465–493, 2007

[3] Daley, S and Johnson, FA and Pearson, JB and Dixon, R, Active vibration control for marine applications, *Control Engineering Practice.* **12**(4): 465–474, 2004

[4] Zhu, WH and Tryggvason, B and Piedboeuf, JC, On active acceleration control of vibration isolation systems, *Control Engineering Practice*, **14**,863–873, 2006

[5] Debnath, N and Dutta, A and Deb, SK, Placement of sensors in operational modal analysis for truss bridges, *Mechanical Systems and Signal Processing* **31**: 196–216, 2012

[6] Gawronski, W, *Advanced structural dynamics and active control of structures.* Springer Verlag, 2004

[7] Kermani, MR and Moallem, M and Patel, RV, Parameter selection and control design for vibration suppression using piezoelectric transducers *Control Engineering Practice*, **12**: 1005–1015, 2004

[8] Pulthasthan, S and Pota, HR, The optimal placement of actuator and sensor for active noise control of sound-structure interaction systems, *Smart Materials and Structures*, **17**(3), 2008

[9] Derham, RC and Hagood, NW, Rotor design using smart materials to actively twist blades, *Proceedings of the American Helicopter Society 52nd Annual Forum.* pp.1242–1252, Washington DC, 1996

[10] Staple, A and Wells, D, The development and testing of an active control of structural response system for the EH101 helicopter *Proceedings of the 16th European Rotorcraft Forum.* **9**, 1990

[11] Sutton, TJ and Eliott, SJ and Brennan, MJ and Heron, KH and Jessop, DAC, Active isolation of multiple structural waves on a helicopter gearbox support strut, *Journal of Sound and Vibration*. **205**(1): 81-101, 1997

[12] Daley, S and Wang, J, A geometric approach to the design of remotely located vibration control systems, *Journal of Sound and Vibration*. **318**(4): 702–714, 2008

[13] Hartnell-Beavis, MC and Swinbanks, MA, Some recent practical and theoretical developments in noise reduction in ships, *Proceedings of the Conference on Vibration and Noise Levels in Ships at the Institute of Marine Engineers*, **21**: 28–38, 1976

[14] Gardonio, P and Elliott, SJ, Modal response of a beam with a sensor-actuator pair for the implementation of velocity feedback control, *Journal of Sound and Vibration*. **284**(1):1–22, 2005

[15] Pope, SA and Daley, S, Redistribution of the energy in a vibration isolation system under the action of discrete frequency active control, *Proceedings of Active*. pp. 149–159, 2009

[16] Zhang, Kai and Scorletti, Gérard and Ichchou, MN and Mieyeville, F, Phase and gain control policies for robust active vibration control of flexible structures, *Smart Materials and Structures*, **22**(7): 075025, 2013

[17] MacMartin, DG and How, JP, Implementation and prevention of unstable optimal compensators, *American Control Conference*. **2**: 2190–2195, 1994

[18] Balini, H and Scherer, C and Witte, J, Performance enhancement for amb systems using unstable $\mathcal{H}_\infty$ controllers, *Control Systems Technology, IEEE Transactions on*. **19**(6): 1479–1492, 2011

[19] Gümüssoy, Suat and Özbay, Hitay, Remarks on strong stabilization and stable $\mathcal{H}_\infty$ controller design, *Automatic Control, IEEE Transactions on*. **50**(12): 2083, 2005

[20] Lee, P.H. and Soh, Y.C., Synthesis of stable $\mathcal{H}_\infty$ controller via the chain scattering framework, *Systems and Control Letters*, **46**: 1968-1972, 2002

[21] Petersen, I, Robust $\mathcal{H}_\infty$ control of an uncertain system via a strict bounded real output feedback controller, *Optimal Control Applications and Methods*. **30**(3): 247–266, 2009

[22] Wang, J and Daley, S, Broad band controller design for remote vibration using a geometric approach, *Journal of Sound and Vibration*. **329**(19): 3888–3897, 2010

[23] Ubaid, U. and Daley, S, and Pope, SA, Broadband design of remotely located vibration control systems: A stable solution for non-minimum phase dynamics, *INTER-NOISE and NOISE-CON Congress and Conference Proceedings* pp. 835–840, 2011

[24] Ferreres, G and Puyou, G, Feasibility of $\mathcal{H}_\infty$ design specifications: an interpolation method, *International Journal of Control*, **78**(12):927–936, 2005

[25] Delsarte, Ph. and Genin, Y. and Kamp, Y, On the role of Nevanlinna-Pick problem in circuit and system theory, *International Journal of Circuit Theory and Applications*. **9**(2), 177-187, 1981

[26] Ubaid, U. and Daley, S, and Pope, SA and Zazas, I, Experimental validation of a geometric method for the design of stable and broadband vibration controllers using a propeller blade test rig, *Control, 2012 UKACC International Conference on* pp. 369–374, 2012

[27] Freudenberg, JS and Hollot, CV and Middleton, RH and Toochinda, V, Fundamental design limitations of the general control configuration, *Automatic Control, IEEE Transactions on*, **48**(8):1355-1370 2003

[28] Freudenberg, JS and Hollot, CV and Middleton, RH, A trade-off between disturbance attenuation and stability robustness, *American Control Conference, Proceedings of* , **6**:4816–4821 2003

[29] Reynolds, P, *The effects of raised access flooring on the vibrational performance of long-span concrete floors*. PhD thesis, University of Sheffield, 2000

[30] Nyawako, DS and Reynolds, P, Response-dependent velocity feedback control for mitigation of human-induced floor vibrations, *Smart Materials and Structures*. **18**(7): 075002, 2009

[31] Przedwojski, M and Daley, S, An $\mathcal{H}_\infty$ design approach to the control of human induced vibration in office floor structures, *20th International Congress on Sound & Vibration*. 2013

[32] Ubaid, U. and Daley, S, and Pope, SA, Design of remotely located stable vibration controllers for non-minimum phase systems, *14th Asia Pacific Vibration Conference*, Hong Kong, 2011